Structures and Growth Mechanisms for Heteroepitaxial fcc(111) Thin Metal Films

ARTICLE *in* THE JOURNAL OF PHYSICAL CHEMISTRY · MAY 1995

Impact Factor: 2.78 · DOI: 10.1021/j100019a051

2 AUTHORS, INCLUDING:

Tsun-mei Chang
University of Wisconsin - Parkside
42 PUBLICATIONS **1,517** CITATIONS

Structures and Growth Mechanisms for Heteroepitaxial fcc(111) Thin Metal Films†

Tsun-Mei Chang‡ and Emily A. Carter*

Department of Chemistry and Biochemistry, University of California, Los Angeles, California 90095-1569

Received: July 30, 1994; In Final Form: January 31, 1995®

We investigate film morphologies of heteroepitaxial face-centered cubic (fcc) thin metal adlayers grown on fcc(111) metal substrates using a statistical-mechanical mean-field theory. In order to develop a general understanding of how various intrinsic properties of the film and substrate dictate the thermodynamically-preferred film structures, fourteen fcc(111)/fcc(111) interfaces with lattice mismatches ranging from −17% to +21% and bulk cohesive energies ranging from 2 to 6 eV/atom are examined. We find that relative magnitudes of lattice mismatch, surface energy, and bulk cohesive energy all contribute to determining the film structures, in contrast to our findings for fcc(100) interfaces, where lattice mismatch played the dominant role. Pseudomorphic growth is predicted to be preferred for small-mismatched interfaces, while incommensurate films are favored for large-mismatched interfaces. When the film has a lower surface energy and bulk cohesive energy than the substrate, layer-by-layer or Stranski−Krastanov growth is favored. Three-dimensional growth becomes dominant for interfaces where the relative surface and bulk cohesive energy of the film is large compared to the substrate. We also find the film structures are insensitive to temperature variations in the range 300−800 K. Finally, our theoretical calculations are in generally excellent agreement with experimentally-determined film structures, and we have gone further to predict the morphological nature of a number of heterointerfaces that have yet to be examined experimentally.

I. Introduction

There has been intense interest in the study of heteroepitaxial ultrathin metallic films for many years.[1−8] The main motivation for these studies is the hope that film properties may be modified strongly by the influence of the substrate, giving rise to a new class of easily created materials with non-bulk-like, non-alloy-like physical and chemical properties. In order to understand and eventually manipulate such properties, one must first be able to characterize the film structures and morphologies.

When adatoms are adsorbed onto a substrate, three major types of thermodynamic growth modes have been observed.[3] One of the growth mechanisms is known as the FM (Frank−van der Merwe) mode, which consists of layer-by-layer growth of the adlayers. Another growth mechanism is VW (Volmer−Weber) growth, describing three-dimensional clustering of adatoms on a bare substrate. SK (Stranski−Krastanov) growth is a mixture of the above two growth modes, which involves three-dimensional clustering after one or a few complete adlayers are formed first. The structure of the films can be distinguished further as pseudomorphic or incommensurate. When adlayers adopt the substrate structure, the film is said to grow pseudomorphically. Incommensurate growth is defined as the case when there are no common basis vectors in the reciprocal lattices of the substrate and the film.[6,9,10]

Many theoretical studies have been devoted to the understanding of growth morphologies of heteroepitaxial interfaces. One phenomenological criterion has been postulated by Bauer to determine the growth mode based on the competition of the surface free energies of the substrate and adlayer and the interfacial free energy.[3] This thermodynamic argument is closely related to Young's equation in wetting theory[11−13] and coincides with physical intuition. However, due to their phenomenological nature, the parameters used there cannot be easily calculated or even defined straightforwardly, complicating its application to real systems.

Another approach relies on total energy calculations.[1,2] By minimizing the system's total energy with respect to the adlayer lattice parameters and the relative position of the substrate to the adlayer, equilibrium film structures can be determined. This approach has been applied to many metal-on-metal systems and yields reasonably accurate predictions.[14] The main drawback of this approach is that the predictions are relevant to zero Kelvin structures only. In practice, it has been shown that temperature can have a significant effect and will indeed change film morphologies.[15,16]

One set of theoretical methods that takes temperature into consideration is computer simulation. Both Monte Carlo (MC) and molecular dynamics (MD) have been used to study heteroepitaxial interfaces.[17−24] These simulations can provide detailed information on the atomic level. However, these simulations are computationally intensive. In order to fully characterize the factors that dictate film morphology and to be computationally efficient, we recently developed a statistical-mechanical theory to study the thermodynamic growth morphologies of heteroepitaxial thin metal overlayers.[25] This approach is based on a mean-field approximation and has been applied to fcc/fcc(100) interfaces. We showed that this theory can capture the essential physical trends and give reasonable predictions for real metal-on-metal systems.[25]

Our goal in our previous and present work was to study a wide variety of systems where we varied relative properties of the film and the substrate and looked for trends that might allow *a priori* predictions of film structures based on structure−property relationships we might establish. For example, clearly, a mismatch in preferred bulk lattice structures between the film and the substrate leads to strain at the interface. Depending on the size of the mismatch, this may result in altered structures for the film. Another property expected to play a role is the intrinsic surface energy of each material. For example, we

† We are happy to dedicate this paper to our wonderful colleague Professor Mostafa El-Sayed on the occasion of his 60th birthday. Mostafa has grown interested in materials science recently, and we hope he finds this materials-related contribution to his liking.

‡ Present address: MSRC, MSIN K1-90, 906 Battelle Blvd., Richland, WA 99352.

® Abstract published in *Advance ACS Abstracts,* May 1, 1995.

0022-3654/95/2099-7637$09.00/0

expect that a low surface energy metal (i.e., a metal for which the energy to create a surface is small) will like to "wet" (i.e., completely cover) a high surface energy metal, leading to, perhaps, layer-by-layer (FM) growth. Finally the other obvious property of these materials to consider is how strong their metal−metal bonds are. In other words, we expect the relative bulk metal cohesive energies (bulk, because it is not possible to measure thin film cohesive energies accurately) to dictate, for example, whether three-dimensional clustering will occur. This would be expected in the case where the metal−metal bonds are stronger in the film than in (or to) the substrate. In our study of fcc metal films grown on fcc(100) substrates,[25] we found that lattice mismatch was by far the dominant factor that determined film morphology. However, we did find that relative surface energies can give rise to subtle modifications in the thermodynamic growth modes. By contrast, relative bulk cohesive energies were not found to correlate at all with the predicted film morphologies. Since fcc(111) is a denser surface than fcc(100), we thought it would be interesting to see how this higher-coordinated substrate surface affects the film morphologies. As we will see, there are significant differences in the influence of the two surfaces.

Many experimental studies on heteroepitaxy have focused on metal overlayers grown on low index surfaces, i.e., (100), (110), (111), due to their relatively simple structures.[26−30] Among the three low-index fcc surfaces, fcc(110) is the least dense surface and often undergoes surface reconstruction in order to increase the number of metal−metal bonds at the surface. Compared to fcc(110), fcc(100) and fcc(111) surfaces are more densely packed and most do not reconstruct. Therefore, it is simpler to study the fcc(100) and fcc(111) interfaces, both experimentally and theoretically, to avoid the complications associated with the major surface rearrangements that occur on the fcc(110) surface. This is why our previous and our current work focused on the former two interfaces. We delay a review of relevant experimental fcc(111) interfacial studies until later, where we make detailed comparisons with our theoretical predictions.

Herein we apply the statistical-mechanical mean-field approach to study fcc metal films grown on fcc(111) metal substrates as a function of film−substrate lattice mismatch, surface and bulk cohesive energies, coverage, and temperature. The goal is to obtain an overall understanding of heteroepitaxial thin film growth, but specifically here to understand the effect of the density of the substrate surface on the resulting film morphologies.

The organization of this paper is as follows. In section II, we describe the mean-field approach and its basic assumptions. The calculational details for real metal-on-metal systems will also be discussed. In section III, we present the mean-field results for fourteen fcc/fcc(111) interfaces. By comparing the relative free energies, the thermodynamic growth morphologies of these systems can be identified. We then compare the results with available experimental studies in section IV. In section V, we conclude.

II. Method

Recently, we developed a statistical-mechanical theory to study heteroepitaxial growth.[25] By employing a mean-field approximation, this approach provides an efficient means for evaluating the free energies of various film structures. By minimizing the free energy, the lowest-energy structure is recognized as the equilibrium structure and the thermodynamic growth mechanism can thus be inferred.

It is well-known that, for a thermodynamic system, once the partition function is evaluated, all thermodynamic information can be obtained. Given a system with M substrate atoms and N adatoms, the partition function can be written simply as

$$Z = \frac{1}{N!M!} \int d\vec{R}_1 \int d\vec{R}_2 \ldots \int d\vec{R}_M \int d\vec{r}_1 \int d\vec{r}_2 \ldots \int d\vec{r}_N \times \exp(-\beta U(\vec{r}_1,\vec{r}_2,\ldots,\vec{r}_N,\vec{R}_1,\ldots,\vec{R}_M)) \quad (1)$$

where U is the system's potential energy that represents a sum over the interactions of all the particles in the system, and $\vec{R}_i$ and $\vec{r}_j$ are the positions of the substrate atom i and adatom j, respectively. In the above, $\beta = 1/k_B T$, where k_B is the Boltzmann constant, and T is the temperature of the system. The factor $1/M!N!$ takes care of the indistinguishability of the particles. Obviously, straightforward evaluation of Z for a macroscopic system is a formidable task. Therefore, it will be useful to approximate this partition function by a simpler form that can be evaluated readily.

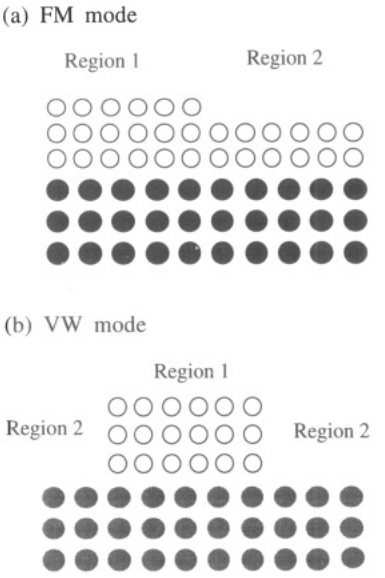

Figure 1. Examples of adatoms (a) growing layer-by-layer and (b) forming three-dimensional clusters on top of a bare substrate. The white and dark circles indicate the adatoms and substrate atoms, respectively.

If we consider these crystalline systems at low to intermediate temperatures far away from their melting points, then it is reasonable to assume that each particle will stay near its equilibrium lattice site. For heteroepitaxial systems, the structures of the substrates and the adlayers may be distorted from their bulk equilibrium structures due to interfacial strain. This deformation can be considered uniform, as suggested by previous MC simulations.[31,32]

Because of the presence of the interface, the translational symmetry in the direction perpendicular to the interface is lost in these systems. Therefore, each particle in each different layer will experience different interatomic interactions from all the other particles in the system. If we assume that edge or boundary effects can be ignored, then one or two regions in each layer can be further identified depending on various growth morphologies. Now, within each region in each layer, the particle possesses translational symmetry in the lateral directions (parallel to the interface) and is considered to be exposed to an averaged atomic environment. In Figure 1, we show examples where adatoms either grow layer-by-layer or form three-dimensional clusters on top of a bare substrate. First, let us consider the case where the adlayers grow in a layer-by-layer manner. If the topmost adlayer partially covers the surface with an area fraction, c, then the two regions can be easily distinguished by the boundary of the topmost adlayer. For the case of three-dimensional growth, if we assume that the clusters are of uniform height and macroscopic size and cover the

substrate surface with a fraction, c, then only one averaged interaction will be experienced by each adatom in each adlayer. However, there are two types of substrate environments, depending on whether adatoms are on top of that portion of substrate.

Suppose there are M_z substrate layers with M_{xy} atoms per layer, N_z adlayers with cN_{xy} adatoms per layer in region 1 and N'_z adlayers with $(1 - c)\,N_{xy}$ adatoms per layer in region 2. Then, assuming that no defects such as vacancies, impurities, and dislocations exist in the system, and with the mean-field approximation, the adlayer–substrate partition function can be written as a product of single particle partition functions:

$$Z_{MF}(a_{ad}, a_{sb}, T) \approx \prod_{\alpha=1}^{M_z}(z^s_{\alpha 1})^{cM_{xy}}(z^s_{\alpha 2})^{(1-c)M_{xy}} \prod_{\beta=1}^{N_z}(z^a_{\beta 1})^{cN_{xy}} \prod_{\beta=1}^{N'_z}(z^a_{\beta 2})^{(1-c)N_{xy}} \quad (2)$$

In the above, $z^s_{\alpha 1(2)}$ and $z^a_{\beta 1(2)}$ are the single particle partition functions of substrate atom, s, and adatom, a, in the αth and βth layers in region 1 (2), respectively. Since now the particles are distinguishable, the constant of $1/N!M!$ is no longer needed. The single particle partition functions are defined as

$$z^s(a_{ad}, a_{sb}, T) = \int_{\Delta_s} d\vec{R}\, \exp(-\beta E_s(\vec{R}, a_{ad}, a_{sb})) \quad (3)$$

$$z^a(a_{ad}, a_{sb}, T) = \int_{\Delta_a} d\vec{r}\, \exp(-\beta E_a(\vec{r}, a_{ad}, a_{sb})) \quad (4)$$

where $E_{s(a)}$ is the interaction energy of the substrate atom (adatom) at position $\vec{R}$ ($\vec{r}$) with all the rest of the particles in the system at their equilibrium positions. The integration is performed over the Wigner–Seitz cell of the substrate atom, Δ_s, and of the adatom, Δ_a, respectively. The substrate and adlayer lattice parameters in the direction parallel to the interface are denoted as a_{sb} and a_{ad}, respectively. When a_{sb} and a_{ad} are changed from their bulk values, the interlayer spacing will also be changed in a manner that will be described later. (The preferred bulk lattice constants of substrate and adatom are denoted as a^*_{sb} and a^*_{ad}, respectively.)

From eq 2, the Helmholtz free energy of the system, A, can be expressed as

$$A(a_{ad}, a_{sb}, T) = -k_B T\Big[cM_{xy}\sum_{\alpha}^{M_z}\ln z^s_{\alpha 1} + (1-c)\,M_{xy}\sum_{\alpha}^{M_z}\ln z^s_{\alpha 2} + cN_{xy}\sum_{\beta}^{N_z}\ln z^a_{\beta 1} + (1-c)\,N_{xy}\sum_{\beta}^{N'_z}\ln z^a_{\beta 2}\Big] \quad (5)$$

From this expression, the free energy of a macroscopic heteroepitaxial film–substrate system can be evaluated easily. By performing a series of free energy calculations for various film structures (as a function of a_{ad} and a_{sb}) and growth mechanisms, the global minimum in the free energies then permits us to identify the equilibrium film structure. The preferred thermodynamic growth mechanism can thus be inferred from relative free energy differences.

In applying this mean-field approach to real metal-on-metal systems, several assumptions have been made to reduce the computational effort. It is obvious that both the substrate and adlayer lattice parameters may be distorted from their bulk values due to the interfacial lattice-mismatch strain energy. Since the substrate is, for all intents and purposes, a three-dimensionally infinite bulk material, we can safely assume that the lattice parameter of the substrate will remain at its bulk value. However, the situation is quite different for the adlayers. The interfacial strain can have a significant effect on the lattice constants of metal overlayers because of their thinness. Therefore, the film lattice parameter is varied in the free energy calculations in order to obtain equilibrium film structures. Note that in eq 5, A is originally a function of a_{ad}, a_{sb}, and T. With the bulk substrate approximation, A becomes a function of a_{ad} and T, and only parametrically depends on a_{sb}. Evidence from previous MC simulations indicates that the deformation of the adlayers can be considered uniform.[31,32] When the adlayers expand (contract) because of the interfacial strain, the interlayer spacing of the adlayers will shorten (lengthen) in order to reduce the lattice strain built in the adlayers, as suggested by MC simulations and experiments.[26,31–33] It was also observed via constant pressure MC simulations that the interlayer spacing is adjusted in a way so as to compensate for the volume change caused by the lateral lattice deformation.[31–33] We therefore adjust the film interlayer lattice spacing accordingly, in order to conserve volume. Note that the particles are not allowed to move in the direction perpendicular to the interface once the interlayer spacing is determined in this manner. Thus, alloy formation at the interface is not considered in this mean-field approximation.

Note that we also have made the assumption that each particle in each region in each layer will experience the same environment. In reality, a mismatch will occur at the heteroepitaxial interface with a periodicity that depends on the structural differences between these two materials. Therefore, near the interface, each particle is subject to different environments and will experience different atomic interactions. This effect is taken into account by averaging the interactions over all the atomic arrangements. This averaging process enables us to only evaluate one averaged particle partition function per region per layer instead of calculating the partition function for every particle in different environments, and hence this greatly reduces the computational effort. The integration over the Wigner–Seitz cell for a single particle partition function is calculated using the algorithm of the extended Simpson's rule with an adjustable step size.[34] When the relative difference between two sequential integrations is less than 0.01%, the results are considered converged.

In order to characterize the thermodynamic growth mechanism of the adlayers, free energies for several ideal configurations that are typical for the three major growth modes are evaluated. It is well-known that, in addition to these three growth modes, more complex growth morphologies (for example, alloy formation and sandwich structures) can also occur in heteroepitaxial interfaces.[35,36] Although it is possible to consider these structures in the mean-field approach, we will focus on only the three most common growth modes in the present work. We recognize that this limits our predictions such that we may be predicting only metastable structures rather than global minimum energy structures in some cases.

We consider a configuration where adatoms form complete layers on top of the substrate, which is representative of layer-by-layer growth. We also consider configurations where adatoms form three-dimensional clusters on top of a bare substrate or on top of a complete adlayer for coverages greater than 1 monolayer (ML, where ML is the unit of coverage and is defined as one adatom per surface substrate atom). These two configurations are typical of VW and SK growth, respectively. It is reasonable to assume that these clusters are of macroscopic size; thus the contribution to the free energy from island boundaries or edges can be neglected. Therefore, only the free energy of the atoms inside the three-dimensional clusters

is calculated. At the end, we compare free energies for various structures containing the same number of substrate atoms and adatoms. The minimum in the free energy will yield predictions of the (perhaps metastable) equilibrium film structures and the thermodynamically preferred growth mechanisms.

Although any type of interaction potential can be used in the mean-field approach, the Rafii−Tabar−Sutton−Chen parametrizations of the Finnis−Sinclair (FS) pseudo-many-body potentials are used to represent the substrate−substrate, substrate−adatom, and adatom−adatom interactions in the present work.[37−39] The potential radial cutoff for this parametrization is at two lattice constants, which is about 7−10 Å for fcc metals. These potentials have been shown to give reasonable predictions for bulk properties of fcc metals and alloys. These potentials have been utilized also to predict properties of metal surfaces and heteroepitaxial interfaces, yielding structures in good agreement with experiment.[40−43] Analysis by Todd and Lynden-Bell[40] suggested that these potentials are adequate for describing the metal−metal bonding in at least a qualitatively correct manner. We have shown also that these FS potentials yield similar predictions to embedded atom method and glue model potentials for epitaxial growth studied via MC simulations.[43] Furthermore, the FS potential has been shown to correctly predict the hexagonal surface reconstruction of Au(100)[43] and the missing row reconstruction of Pt(110) surfaces.[44] These results suggest that complex surface properties of FS-described metals are reasonable.

In our analysis of the mean-field results, the numerical values of surface energies of the fcc metals are invoked in order to fully characterize the film growth morphologies. Here, the surface energy is calculated by taking half of the energy difference between the potential energy of a three-dimensional bulk crystal with periodic boundary conditions applied in all three directions and the potential energy of this crystal with periodic boundary conditions removed in one direction (which creates two surfaces). Note that because we do not consider surface relaxation, the surface energies calculated here may be upper bounds for the true surface energies. (Surface relaxation is unimportant here because adsorption of the film tends to lift any surface reconstruction of the bare substrate.[45]) Note that recently Raeker and DePristo[46] have developed an alternative method for calculating the surface and interfacial energies based on a similar idea. These quantities are shown to be useful in characterizing film morphologies. However, their formula is restricted to pseudomorphic adlayers and is only valid at 0 K.

III. Results and Discussion

We studied fourteen heteroepitaxial fcc/fcc(111) interfaces with substrate−film lattice mismatches ranging from −17% to +21% and metals with bulk cohesive energies ranging from 2 to 6 eV/atom. The lattice mismatch parameter is defined as $(a^*_{ad}/a^*_{sb} - 1) \times 100\%$; thus positive mismatches indicate that a^*_{ad} is greater than a^*_{sb}. We have been careful to choose only metal pairs for which no evidence exists for alloy formation within thin films at the temperatures of interest. Although some of the chosen metal pairs do form bulk alloys, e.g., Pt/Rh, no studies have been reported indicating alloy formation for a thin film of either Pt on Rh(111) or Rh on Pt(111). Another graphic example of the differences that can occur between what one expects from bulk thermodynamics and what one finds for thin film thermodynamics is provided by Au films on Cu(111). While Au and Cu certainly form stable bulk alloys, Au deposited on Cu(111) at room temperature does not alloy and only at very high temperatures does Au intermix with the Cu.[35] Therefore, we can safely proceed under the assumption our model adopts of no alloying for the systems we discuss below.

We have investigated the effects of lattice mismatch, surface and bulk cohesive energies, coverage, and temperature on heteroepitaxial thin fcc(111) film growth. The results will be compared to our findings for thin films grown on fcc(100) substrates in order to characterize the role played by substrate lattice symmetry/density. Since epitaxial growth typically is carried out at temperatures at or above room temperature, we evaluated the film structures at $T = 300$ and 800 K.

In the following figures, the results of calculated film−substrate free energy curves at 300 K are shown as a function of film parallel lattice parameter, $a_{||}$, for the various film morphologies described earlier. The metal films are all taken to have fcc(111) symmetry, with the high symmetry axes parallel to that of the substrates'. We normalize the numerical value of the free energy, A, by the number of surface substrate atoms (by setting $M_{xy} = 1$ in eq 5), and thus it is in units of electronvolts per surface substrate atom. Recall that the Finnis−Sinclair potentials have a radial potential cutoff at two lattice constants. As a result of this cutoff, the substrate atoms that are more than two lattice constants below the interface will not be affected by the presence of the adlayers. The free energy associated with these substrate atoms therefore will be the same for different film structures and will only add a constant contribution to the system's total free energy. Therefore, we need not (and do not) calculate their contribution to the total free energy, since we are only interested in relative free energies anyway. Because of this potential cutoff, the numerical values of free energies (which have been normalized by the number of surface substrate atoms), reported in Figures 2−7, correspond to the sum of free energies associated with four or five substrate atoms and a number of adatoms that depends on the coverage. For example, at a coverage of 1 ML, the free energy is for one adatom and four or five substrate atoms. The labels FM in the figure captions refer to the free energy curves for layer-by-layer (FM) growth. The labels VW(n) describe adatoms forming three-dimensional clusters n layers thick on top of a bare substrate, corresponding to three-dimensional (VW) growth. The labels SK(n) represent the SK growth mode with adatoms forming three-dimensional n-layer clusters on top of one complete adlayer. Note that when the adlayers adopt the bulk lattice constant of the substrate (corresponding to pseudomorphic growth), the interfacial strain will be minimized. Thus, a sharp dip, corresponding to at least a local minimum, is expected in the free energy curves at the substrate lattice constant in the following figures. We now display several illustrative examples of heteroepitaxial metallic interfaces, with the results from all fourteen systems discussed later.

In Figure 2a,b, we show the free energy curves for Pt grown on Rh(111) as a function of film parallel lattice constant at coverages of 0.9 and 1.5 ML, respectively. This interface is characterized by a lattice mismatch of 3.16%. For small mismatched interfaces, it is expected that pseudomorphic growth will be favorable. Indeed, we observe that the free energy global minimum lies at the bulk Rh lattice constant of 3.80 Å, indicating that Pt grows pseudomorphically with the substrate. Note that Pt has a much lower surface energy than Rh (see Table 1). Since surface energy determines the tendency for a metal to cover (wet) the surface, we expect that layer-by-layer growth should be energetically favored. Indeed, it is clear from the free energy curves in Figure 2a that pseudomorphic FM growth has a substantially lower free energy than pseudomorphic VW growth (by 0.17 eV/atom) at submonolayer coverages, while Figure 2b suggests that pseudomorphic SK growth is slightly higher (by 0.01 eV/atom) in free energy than FM growth for multilayer coverages. Thus, Pt prefers to form complete adlayers instead of three-dimensional clusters at coverages up

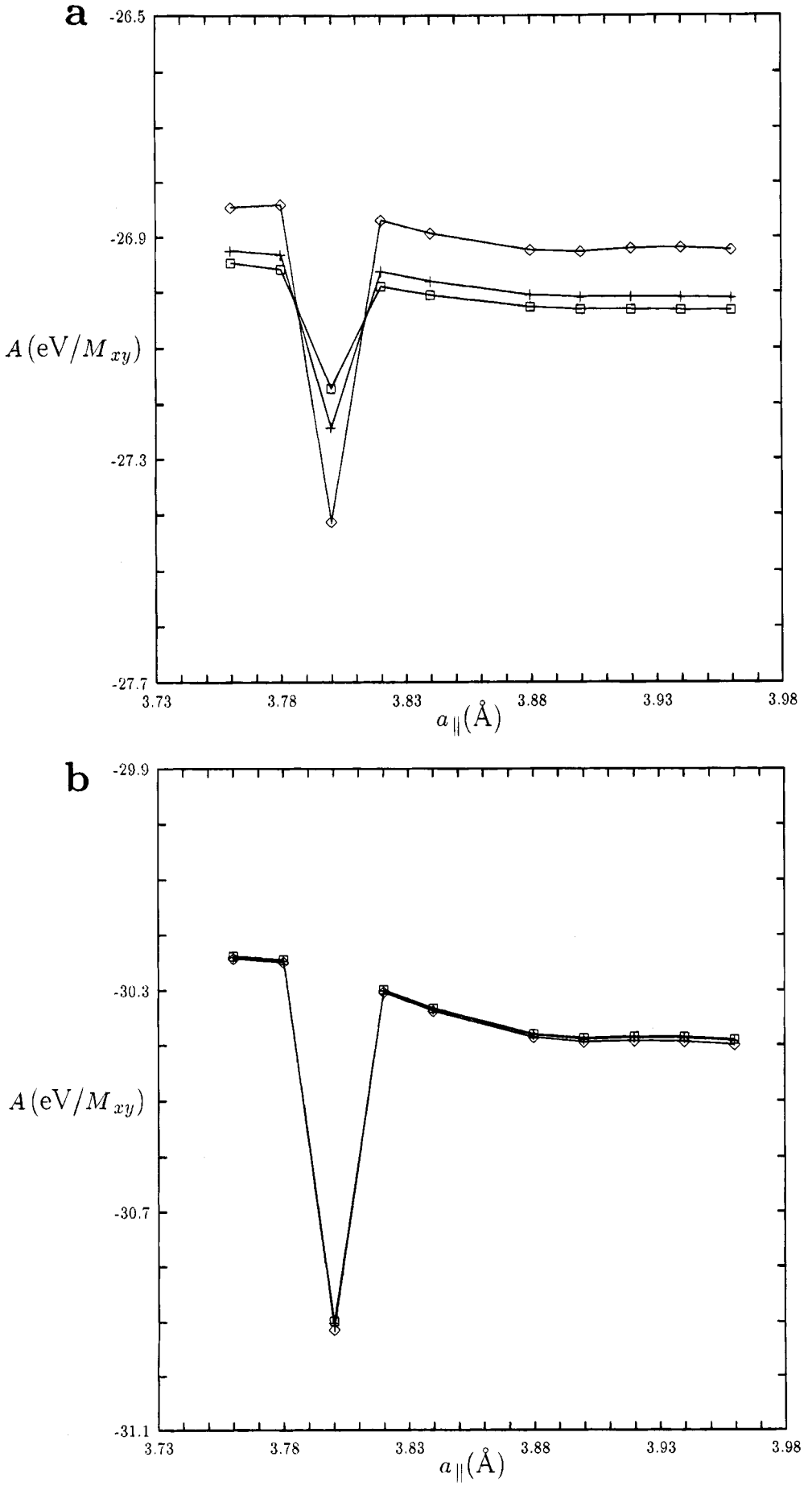

Figure 2. Free energies (eV/M_{xy} = eV/surface substrate atom) as a function of the adlayer parallel lattice spacing ($a_{||}$, Å) for Pt grown on Rh(111) at 300 K, for Θ_{Pt} = (a) 0.9 ML and (b) 1.5 ML. In a, ◇, +, and □ correspond to the free energies for FM, VW(2), and VW(3) growth, respectively. In b, ◇, +, and □ correspond to FM, SK(2), and SK(3) growth, respectively. See section III for definitions of FM, VW(n), and SK(n) growth modes.

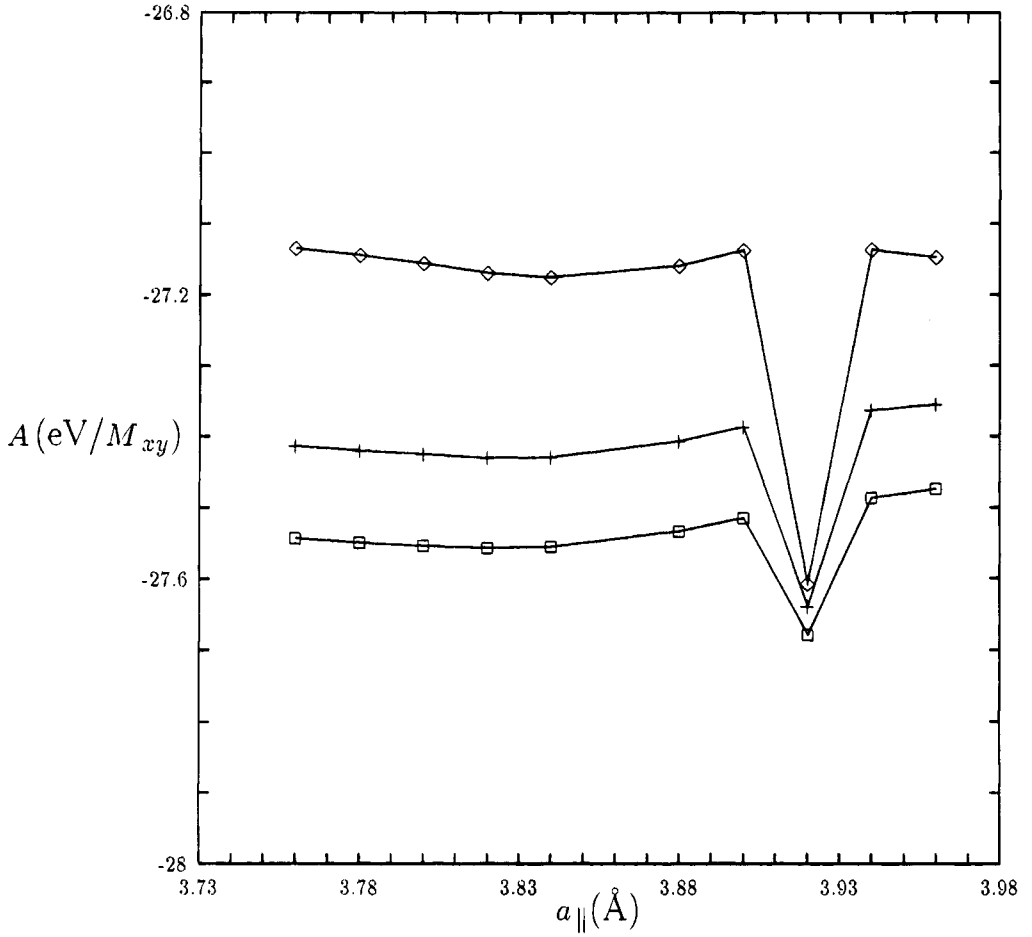

Figure 3. Free energies (eV/M_{xy}) as a function of the adlayer parallel lattice spacing ($a_{\|}$, Å) for Rh grown on Pt(111) at 300 K, for $\Theta_{Rh} = 0.9$ ML. ◇, +, and □ correspond to the free energies for FM, VW(2), and VW(3) growth, respectively.

to at least 2 ML. Thus, we predict that pseudomorphic layer-by-layer growth is the thermodynamically preferred growth morphology for Pt grown on Rh(111).

In Figure 3, we show the reverse case of Rh grown on Pt-(111) at a coverage of 0.9 ML. The lattice mismatch for this interface is −3.06%. For Rh coverages up to 2 ML, it is found that the preferred growth mechanism and film structure are independent of the coverage. For this small mismatched interface, we find that the free energy is the lowest at the bulk Pt lattice constant of 3.92 Å, suggesting again that pseudomorphic growth is preferred. However, since Rh has a much higher surface energy than Pt (see Table 1), Rh prefers to form three-dimensional clusters on top of Pt(111), as indicated by VW growth having significantly lower free energies than FM growth. Thus, we predict that in the thermodynamic limit, Rh will form three dimensional, pseudomorphic clusters on top of Pt(111). The total free energy of the system is minimized by exposing the lower energy surface via three-dimensional clustering of Rh.

In Figure 4a,b, we show the free energy curves for Ni grown on Rh(111) at coverages of 0.9 and 1.5 ML, respectively. This interface is characterized by an intermediate lattice mismatch of −7.37%. For coverages up to 2 ML, we find that Ni adopts the Rh bulk lattice constant of 3.80 Å, indicating that the film grows pseudomorphically, choosing to minimize the interfacial strain at the expense of some strain within the film. As in the case of Pt, Ni has a much lower surface energy than Rh (see Table 1), and hence Ni has a strong tendency to cover the Rh surface. As a result, FM growth again prevails with lower free energies than VW and SK growth by 0.07 eV/atom for submonolayer coverages and by 0.01 eV/atom for multilayer coverages, respectively. Thus, we predict that pseudomorphic FM growth is the thermodynamically favored growth mechanism for Ni grown on Rh(111).

Figure 5 displays the free energy curves for Rh grown on Ni(111) at a coverage of 0.9 ML. In this case, the lattice mismatch is 7.95%. We find that, up to 2 ML, the film morphology does not change with coverage. We observe that although a local minimum occurs at the pseudomorphic lattice parameter of 3.52 Å, the global free energy lies close to the Rh bulk lattice constant of 3.80 Å, leading to an incommensurate overlayer structure. It is obvious from the free energy curves that VW growth has lower free energies than FM growth, suggesting that incommensurate three-dimensional growth is thermodynamically more favorable for Rh grown on Ni(111). This VW growth mechanism is expected since Rh has a very high surface energy, and hence Rh has a strong tendency to cluster on top of a Ni surface.

In Figure 6, we present the results of Ag grown on Pb(111) with a large lattice mismatch of −17.37%. Although only the free energy curves at 0.9 ML are shown, the film morphology remains unchanged for coverages up to 2 ML. In this case, due to the extreme lattice mismatch, Ag prefers to remain in its bulk lattice structure, yielding incommensurate adlayers. The interfacial strain imposed by the incommensurate interface is much less than the intralayer strain that would be present for a pseudomorphic interface, as evidenced by the large difference in free energy for the pseudomorphic versus incommensurate structures in Figure 6. At all coverages, the free energies of VW growth are lower than those of FM growth, suggesting that Ag forms three-dimensional clusters on top of Pb. Again, the relatively higher surface energy of Ag compared to Pb leads to

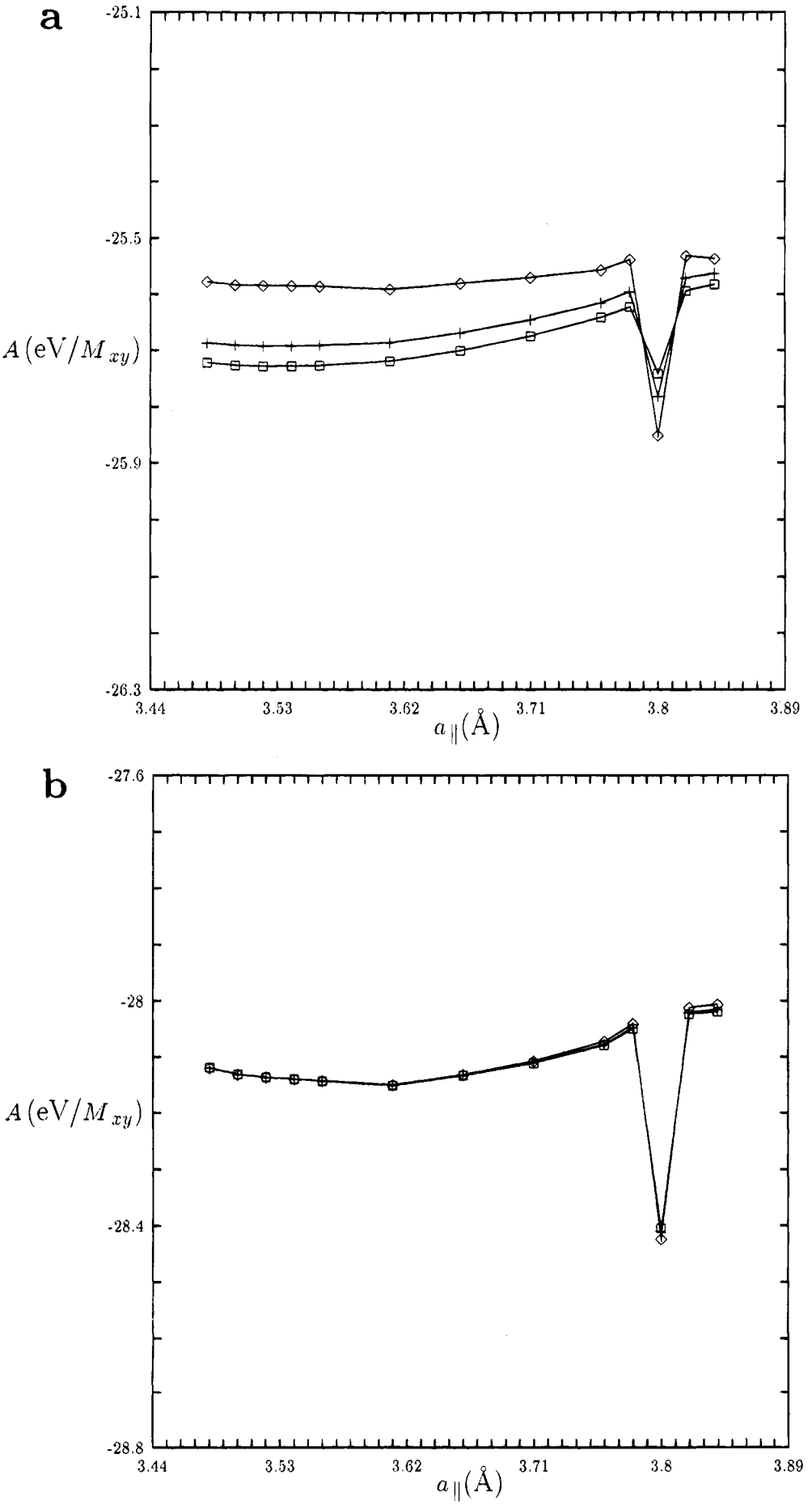

Figure 4. Free energies (eV/M_{xy}) as a function of the adlayer parallel lattice spacing ($a_{\|}$, Å) for Ni grown on Rh(111) at 300 K, for Θ_{Ni} = (a) 0.9 ML and (b) 1.5 ML. In a, ◇, +, and □ correspond to the free energies for FM, VW(2), and VW(3) growth, respectively. In b, ◇, +, and □ correspond to FM, SK(2), and SK(3) growth, respectively.

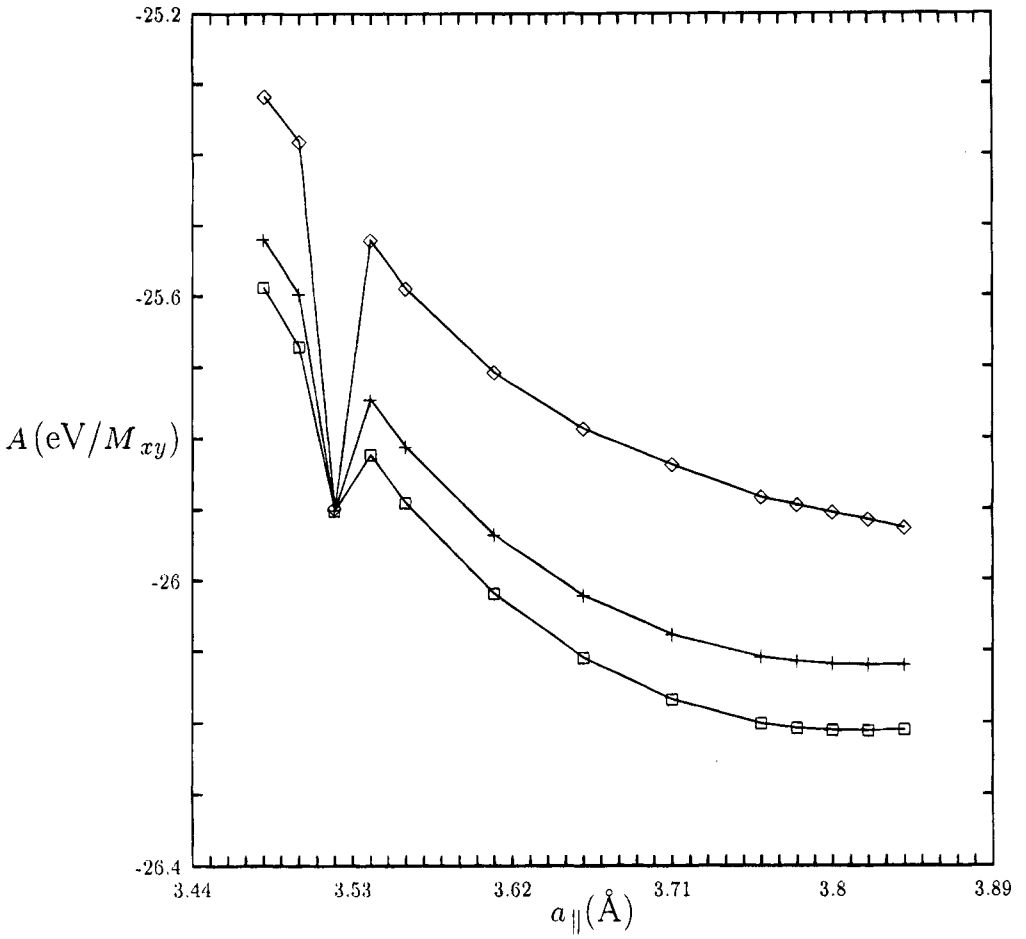

Figure 5. Free energies (eV/M_{xy}) as a function of the adlayer parallel lattice spacing ($a_{\|}$, Å) for Rh grown on Ni(111) at 300 K, for Θ_{Rh} = 0.9 ML. ◇, +, and □ correspond to the free energies for FM, VW(2), and VW(3) growth, respectively.

clustering. Thus, we conclude that incommensurate VW growth is the thermodynamically preferred film morphology for Ag on Pb(111).

Parts a and b of Figure 7 display free energy curves for Pb grown on Ag(111) at coverages of 0.9 and 1.5 ML, respectively. The lattice mismatch for this interface is 21.03%. As clearly shown from the free energy curves, the global free energy minimum lies close to the Pb lattice constant of 4.95 Å, demonstrating again that, not surprisingly, incommensurate growth is found for large mismatched interfaces. Pb is so much larger than Ag that it is impossible to compress Pb into a pseudomorphic structure. At submonolayer coverages, it is more favorable for Pb to fill in the first layer instead of forming three-dimensional clusters, as expected from the fact that Pb has a much lower surface energy compared to Ag. As the coverage exceeds 1 ML, the free energy minima for FM and SK growth are essentially indistinguishable (within 0.003 eV/atom). Thus, we predict that incommensurate SK growth is competitive with incommensurate FM growth for Pb films on Ag(111).

In the above figures, several examples were given to demonstrate how the thermodynamical growth morphology is determined from the free energy curves. In Table 2, a summary is given for the preferred growth morphologies of all the substrate−film interfaces examined. We see from Table 2 that while lattice mismatch is a major factor in determining whether the film grows pseudomorphically with the substrate, the relative surface and cohesive energies also are strong predictors of the growth morphology. For substrate−film lattice mismatches in the range of +7.63 to −7.37%, we generally find that the adatoms form pseudomorphic overlayers. Pseudomorphic growth is favored because the interfacial strain is minimized at the expense of a smaller intraadlayer lattice strain when the films adopt the substrate structures. The one exception is for Rh grown on Ag(111) with a lattice mismatch of −7.09%, which is probably very close to the critical mismatch for pseudomorphic growth. Since Rh has roughly double the surface energy and bulk cohesive energy of Ag (see Table 1), strong Rh−Rh bonds drive the formation of a compressed overlayer. Contrast this with Ni grown on Rh, which has a slightly higher lattice strain (−7.37% mismatch) but grows pseudomorphically. Ni has a much smaller cohesive energy than Rh; thus the driving force toward an incommensurate structure is much less, and therefore Ni on Rh stays pseudomorphic. As the lattice mismatch increases, more and more intrafilm lattice strain builds up in the pseudomorphic adlayers. At a large enough lattice mismatch, the gain in minimizing the interfacial strain is not enough to compensate for the intrafilm lattice strain. At this point, the adlayer will relax toward its bulk lattice structure, leading to incommensurate growth. This happens for lattice mismatches above ~±8% on fcc(111) surfaces (see Table 2).

The growth morphology (FM versus SK versus VW) is determined by all three properties: lattice mismatch, relative surface energies, and relative bulk cohesive energies. In general, for small mismatched interfaces, when the surface and bulk cohesive energies of the film are smaller than the substrate, the preferred thermodynamic growth mechanism is FM or SK growth. This tendency for FM or SK growth can be understood by realizing that these small mismatched systems resemble homoepitaxial interfaces whose growth mechanism is the FM mode in the thermodynamic limit.[47] However, when the surface and characteristic bulk cohesive energies of the adlayer are higher than those of the substrate, the growth morphology will switch to three-dimensional growth, as will be discussed later.

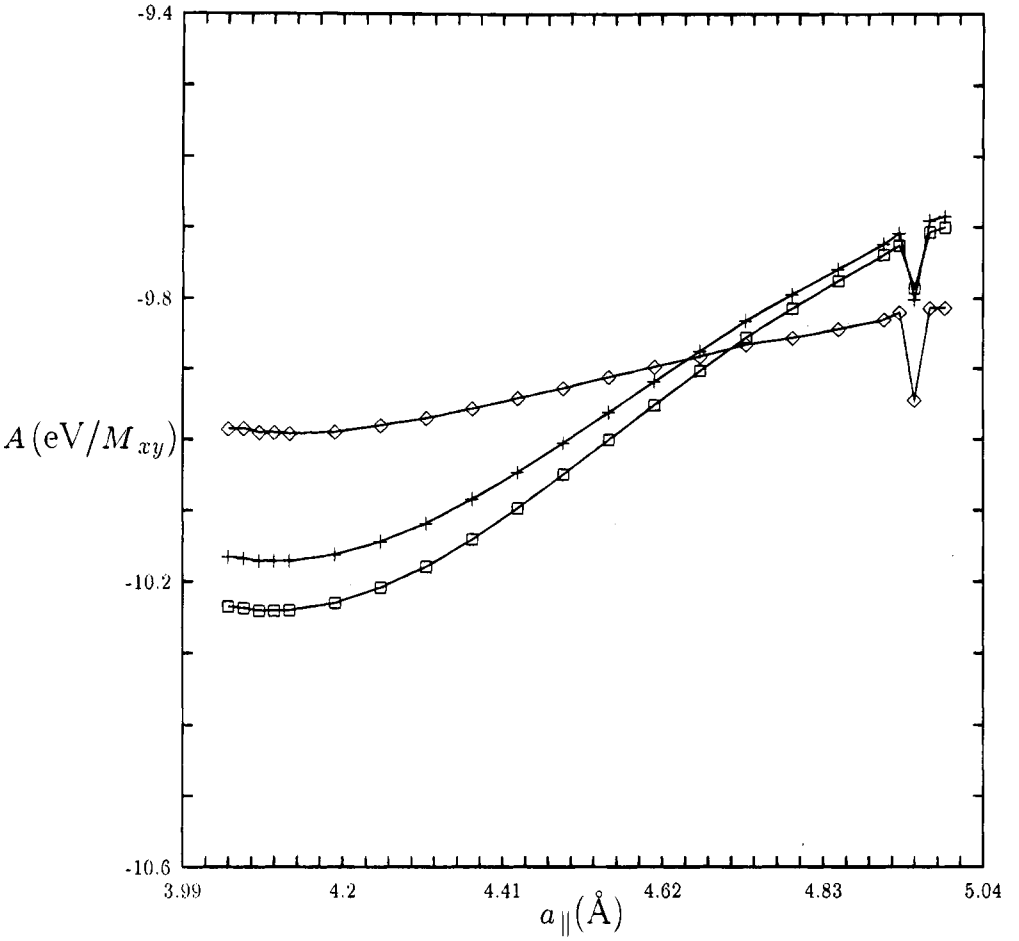

Figure 6. Free energies (eV/M_{xy}) as a function of the adlayer parallel lattice spacing ($a_{\|}$, Å) for Ag grown on Pb(111) at 300 K, for $\Theta_{Ag} = 0.9$ ML. ◇, +, and □ correspond to the free energies for FM, VW(2), and VW(3) growth, respectively.

For large mismatched interfaces, since the preferred structures of the films become incommensurate, the adatoms often form three-dimensional clusters in order to relieve the interfacial strain, leading to VW growth. Pb grown on Ag(111), with a 21.03% lattice mismatch, is the one exception in Table 2. This discrepancy can be explained on the basis of relative surface energies. Since Pb has a much lower surface energy than Ag, Pb has a stronger tendency to wet the Ag surface, favoring FM or SK growth. Surface energies can also explain why Ni grown on Rh(111), with a −7.37% lattice mismatch similar to the −7.09% mismatch of Rh on Ag(111), prefers FM growth rather than VW growth. The high Rh surface energy favors wetting by Ni to lower the overall free energy.

A correlation is clearly observed in Table 2 between the thermodynamic growth mode and the ratio of film to substrate cohesive energy. Since the bulk cohesive energy measures the strength of the metal−metal bonds, if the film has a higher cohesive energy than the substrate, it is expected that the adatoms will prefer to form three-dimensional clusters in order to increase the number of stronger metal−metal bonds. Thus, three-dimensional (VW) growth is favored for most cases examined in Table 2 where the film has a larger bulk cohesive energy than the substrate. However, the situation for the case of Pt grown on Rh(111) is more complicated. Since Pt has a much lower surface energy than Rh (the effect of the surface energy on film morphology will be discussed next), Pt tends to cover the Rh surface. On the basis of surface energy considerations, Pt should grow layer-by-layer on top of Rh(111).

Because the surface energy dictates the tendency for a metal to cover (wet) surfaces, it has a significant effect on growth morphologies. In Table 1, we list the numerical values of the surface energies of fcc metals using Finnis−Sinclair potentials. (Although these surface energies are upper bounds for the true surface energies, the surface energies calculated with surface relaxation[40] via computer simulations are at most 10% lower than the values reported here.) When the adlayer has a surface energy that is less than or equal to that of the substrate, it is energetically favorable for adatoms to cover (wet) the bare substrate in order to reduce the surface energy, which leads to FM or SK growth. Indeed, we see from Table 2 that interfaces with film to substrate surface energy ratios less than unity follow primarily FM or SK growth. For interfaces where the surface energy of the metal overlayer is larger than that of the substrate, the preferred thermodynamic growth mechanism switches to three-dimensional (VW) growth. One exception is found for the case of Au grown on Cu(111). Since Au has a slightly higher bulk cohesive energy than Cu, and the lattice strain for this interface is extremely large (13.02% mismatch), it is conceivable that Au may want to form three-dimensional clusters on top of Cu(111) in order to reduce interfacial strain and gain more Au−Au bonds. Clearly, there is a delicate balance between the surface and cohesive energy driving forces. Experimentally, Au has been observed to follow incommensurate, VW growth on Cu(111) at room temperature.[35,48]

We were interested in determining whether modest temperature changes would affect film structural charactistics. We therefore examined several interfaces: Pt on Rh(111), Rh on Pt(111), Ag on Rh(111), Rh on Ag(111), Ni on Rh(111), Rh on Ni(111), Ag on Pb(111), and Pb on Ag(111) at a higher temperature, 800 K. Although temperature is known for some interfaces to produce morphology changes, we find for the cases studied here that temperature does not alter the film structures and growth mechanisms over the temperature range we examined (300−800 K). We might expect that, at lower tempera-

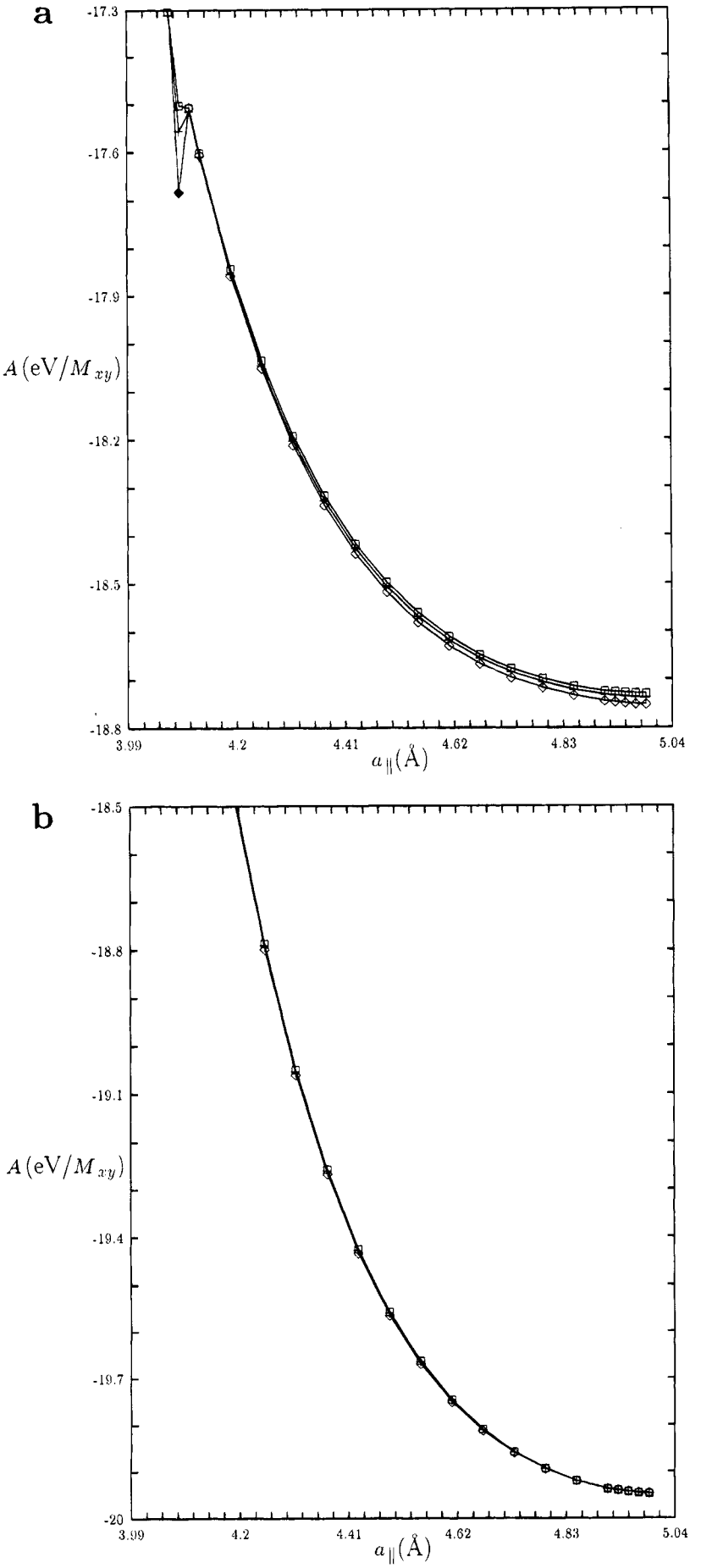

Figure 7. Free energies (eV/M_{xy}) as a function of the adlayer parallel lattice spacing ($a_{\|}$, Å) for Pb grown on Ag(111) at 300 K, for Θ_{Pb} = (a) 0.9 ML and (b) 1.5 ML. In a ◇, +, and □ correspond to the free energies for FM, VW(2), and VW(3) growth, respectively. In b, ◇, +, and □ correspond to the free energies for FM, SK(2), and SK(3) growth, respectively.

TABLE 1: Bulk Lattice Constants (Å), Surface Energies (eV/atom), and Bulk Cohesive Energies (eV/atom) for the Perfect (111) Surfaces of fcc Metals

system	bulk lattice contant[a]	surface energy[b]	bulk cohesive energy[c]
Rh	3.80	0.74	5.75 (5.75)
Ni	3.52	0.48	4.44 (4.44)
Pd	3.89	0.42	3.94 (3.89)
Pt	3.92	0.40	5.86 (5.84)
Cu	3.61	0.38	3.50 (3.49)
Ag	4.09	0.38	2.96 (2.95)
Au	4.08	0.26	3.78 (3.81)
Pb	4.95	0.19	2.04 (2.03)

[a] Taken from: Kittel, C. *Introduction to Solid State Physics*, Wiley: New York, 1986; p 23. [b] Energy of formation of a (111) surface. See text for details. [c] Bulk cohesive energies are calculated using Finnis–Sinclair potentials, and the experimental values are in parentheses [from: Kittel, C. *Introduction to Solid State Physics*; Wiley: New York, 1986; p 55]. Slight discrepancies exist because the Finnis–Sinclair potentials were fitted to earlier experimental data taken from: Kittel, C. *Introduction to Solid State Physics*; Wiley: New York, 1971.

TABLE 2: Summary of Predicted Thermodynamically Preferred Growth Modes and Structures of Heteroepitaxial fcc Metal Films on fcc(111) Metal Substrates, as a Function of Lattice Mismatch, Cohesive Energy, and Surface Energy

system[a]	% lattice mismatch[b]	ratio of E_{coh}[c]	ratio of E_{surf}[d]	growth mode[e]	P/I[f]
Pb/Ag	21.03	0.69	0.50	FM/SK (SK)[53]	I(I)
Au/Cu	13.02	1.08	0.68	VW (VW)[35,48]	I(I)
Rh/Ni	7.95	1.30	1.54	VW	I
Ag/Rh	7.63	0.51	0.51	FM	P
Ag/Pt	4.34	0.51	0.95	SK (FM/SK)[51,52]	P(P)
Au/Pt	4.08	0.65	0.65	FM/SK	P
Pt/Rh	3.16	1.02	0.54	FM	P
Pd/Pt	−0.77	0.67	1.05	FM/SK (FM)[28]	P(P)
Rh/Pt	−3.06	0.98	1.85	VW	P
Pt/Au	−3.92	1.55	1.54	VW	P
Rh/Ag	−7.09	1.94	1.95	VW	I
Ni/Rh	−7.37	0.77	0.65	FM	P
Cu/Au	−11.52	0.93	1.46	VW (SK)[48]	I(I)
Ag/Pb	−17.37	1.45	2.00	VW (VW)[30]	I(I)

[a] These results are independent of temperature over the range 300–800 K. "System" lists the film metal first and the substrate metal second. [b] Lattice mismatch = $(a^*_{ad}/a^*_{sb} - 1) \times 100\%$, where a^*_{ad} and a^*_{sb} are the bulk lattice constants of the metal in the adlayer film and the metal in the substrate, respectively. [c] E_{coh} is the bulk cohesive energy of the metal. The ratio is for the film E_{coh} to substrate E_{coh}. [d] E_{surf} is the calculated surface energy of the metal. The ratio is for the film E_{surf} to substrate E_{surf}. [e] Thermodynamic growth mechanism: FM = layer by layer, VW = three-dimensional clustering, SK = mixture of FM and VW (see text). FM/SK means the two modes are competitive. The available experimental results are given in parentheses. [f] P/I classifies the metal film as growing pseudomorphically (P) or incommensurately (I) on top of the substrate metal. The available experimental results are given in parentheses.

tures, the morphology of these heteroepitaxial interfaces may indeed become temperature dependent due to the lack of thermal fluctuations.[25] However, since most of the experiments on heteroepitaxy are carried out above room temperature, we did not concern ourselves here with film morphologies at lower temperatures.

Previously, we applied this mean-field theory to study the thermodynamic growth morphologies for fcc metal thin films grown on fcc(100) metal substrates. In contrast to the results presented here, we concluded that lattice mismatch dominated the determination of equilibrium film structures, although the surface energy could slightly modify the growth mechanism. We further found that the trends in bulk cohesive energies did not correlate with the film morphologies at all. In the current study, we show for heteroepitaxial fcc/fcc(111) interfaces that although lattice mismatch is still the major factor dictating whether the film grows pseudomorphically with the substrate, lattice strain, surface energy, and the bulk cohesive energy all have significant roles to play in determining the thermodynamic growth mechanism (layer-by-layer versus clustering, etc.). It is intriguing that different physical trends are observed for fcc thin metal overlayers grown on different crystal surfaces of the same fcc metal substrate. We attribute the differences in film morphologies to the fact that fcc(111) is a more densely-packed surface than fcc(100), which emphasizes the role played by enhanced metal–metal bonding (i.e., surface and cohesive energies).

IV. Comparison to Experimental Work

The morphologies of many heteroepitaxial fcc/fcc(111) interfaces have been investigated using experimental techniques such as Auger electron spectroscopy (AES), low-energy electron diffraction (LEED), forward scattering, and scanning tunneling microscopy (STM). For small mismatched film–substrate systems, for example, Pd films on Pt(111) (with a lattice mismatch of −0.77%),[28] Al films on Ag(111) (0.9% mismatch),[29,49] Ag films on Pd(111) (5.14% mismatch),[50] Ag and Au films on Pt(111) (4.34% and 4.08% mismatch, respectively),[51] and Cu films on Pt(111) (−7.91% mismatch),[52] it is found that the adlayers prefer to grow pseudomorphically with the substrate. These observations are in excellent agreement with the present mean-field calculations. Indeed, for all cases with which we can directly compare (see Table 2, rightmost column), we are in complete agreement about the commensurability of the film. Using AES and LEED, Han et al. found that Pd grows layer-by-layer on Pt(111),[28] consistent with the mean-field results. For Ag grown on Pt(111), Davies et al. observed an SK growth mode for Ag overlayers.[51] Later, Schmiedeskamp et al. found that Ag films grow almost layer-by-layer on top of Pt(111); however, they also suspect that a new layer begins to form before the previous layer is completed.[52] These results agree reasonably well with the mean-field calculations.

For film–substrate systems with large lattice mismatch, it is observed experimentally that adatoms will not adopt the substrate structures, leading to the conclusion that pseudomorphic growth is not thermodynamically favored for large mismatched interfaces due to the large adlayer lattice strain. Examples of such interfaces include Cu grown on Au(111) (−11.52% mismatch),[48] Au grown on Cu(111) (+13.02% mismatch),[48] Pb grown on Ag(111) (+21.03% mismatch)[53] and Cu(111) (+37.12% mismatch),[54,55] and Ag grown on Pb(111) (−17.37% mismatch).[30] Again, this general conclusion is consistent with the results from our mean-field theory. Using reflection high-energy electron diffraction (RHEED) and transmission electron microscopy (TEM), Macur and Vook characterized the growth mechanism of Au on Cu(111) as VW growth,[48] in agreement with the mean-field prediction. However, these authors observed SK growth for Cu grown on Au(111) rather than VW growth predicted in the present work. From their RHEED data, they suspect that the adlayers are slightly rotated with respect to the substrate. Thus, the discrepancy in the growth mode may come from the fact that we did not consider rotations of the lattice in our mean-field calculations. Later LEED data of Xu et al.[35] showed that Au grown on Cu(111) at room temperature grows incommensurately with a nearest-neighbor spacing of bulk Au, consistent with our mean-field results. For Ag grown on Pb(111), Takayanagi[30] observed a VW growth mechanism, and, for the reverse case of Pb grown on Ag(111), Takayanagi et al.[53] found an SK growth mode for the adlayers via AES and LEED. These findings are confirmed by the present mean-field predictions.

V. Conclusions

In this work, a statistical-mechanical mean-field formalism has been used to study the heteroepitaxy of strained fcc metal films grown on fcc(111) metal substrates. In order to obtain a global understanding of the physical factors that dictate film growth, we examined the effect of lattice mismatch, surface energies, bulk cohesive energies, coverage, and temperature on film morphology.

It is found that lattice mismatch is the major factor that determines whether the film adopts the lattice structure of the substrate. For small mismatched interfaces, the preferred equilibrium film structures are found to be pseudomorphic with the substrates, while incommensurate film structures are favored for large mismatched systems. By contrast, we conclude that lattice mismatch, bulk cohesive energy, and surface energy are all extremely important in determining the thermodynamic growth mechanism. Generally, small lattice mismatch enhances the chances for layer-by-layer or SK growth, while large lattice mismatch often results in three-dimensional clustering to relieve intrafilm strain that would be present in a flat film.

The relative bulk cohesive energies provide a measure of the metal−metal bond strengths. When the adlayer has a higher characteristic bulk cohesive energy than the substrate, the adatoms will tend to cluster on top of the substrate in order to increase the quantity of stronger metal−metal bonds. Thus, interfaces with high ratios of film to substrate bulk cohesive energies will primarily follow VW growth.

Since the surface energy quantifies the tendency for a metal to wet the substrate, then when the film has a much higher surface energy than the substrate, again three-dimensional growth will minimize the total free energy. Likewise, when the film has a substantially smaller surface energy than the substrate, even with a large lattice mismatch, one can expect complete wetting of the surface by the adlayer.

We have found that these predictions and analyses concerning the film morphologies of these fcc/fcc(111) interfaces are independent of temperature in the range 300−800 K, as was found for fcc/fcc(100) interfaces previously. However, since the fcc(111) surface is denser than the fcc(100) surface, we found that properties related to metal−metal bonding (cohesive and surface energies) play more dominant roles than in the case of the fcc(100) surface. This indicates that the density of the substrate surface can indeed affect film morphologies.

Finally, our mean-field results are generally in excellent agreement with available experimental findings, except in one case where the mean-field theory did not consider a complicated rotation of the film with respect to the substrate. This generally good agreement lends confidence in the method for reliably predicting both film commensurability and film growth mechanisms for systems yet to be studied by experiment. Table 2 provides eight predictions of heteroepitaxial fcc/fcc(111) film structures where we await experimental verification.

Acknowledgment. We are grateful to the Office of Naval Research for primary support of this research. E.A.C. also knowledges the National Science Foundation, The Camille and Henry Dreyfus Foundation, the Alfred P. Sloan Foundation, Union Carbide, and Olin Chemical for support via Presidential Young Investigator, Teacher−Scholar, Research Fellow, Innovation Recognition, and Young Investigator Awards, respectively.

References and Notes

(1) Frank, F. C.; van der Merwe, J. H. *Proc. R. Soc. London* **1949**, *A198*, 205.
(2) Frank, F. C.; van der Merwe, J. H. *Proc. R. Soc. London* **1949**, *A198*, 216.
(3) Bauer, E. *Appl. Surf. Sci.* **1982**, *11/12*, 479.
(4) Cabrera, N. *Surf. Sci.* **1964**, *2*, 320.
(5) Matthews, J. W., Ed. *Epitaxial Growth*; Academic Press: New York, 1975.
(6) Markov, I.; Stoyanov, S. *Contemp. Phys.* **1987**, *28*, 267.
(7) Stoyanov, S. *Surf. Sci.* **1988**, *199*, 226.
(8) Campbell, C. T. *Annu. Rev. Phys. Chem.* **1990**, *41*, 775.
(9) Stoyanov, S. *Surf. Sci.* **1986**, *172*, 198.
(10) Novaco, A. D.; McTague, J. P. *Phys. Rev. Lett.* **1977**, *22*, 1286.
(11) Matthews, J. W.; Jackson, D. C.; Chambers, A. *Thin Solid Films* **1975**, *26*, 129.
(12) Dash, J. G. *Phys. Rev. B* **1977**, *15*, 3136.
(13) Huse, D. A. *Phys. Rev. B* **1984**, *29*, 6985.
(14) Dodson, B. W. *Surf. Sci.* **1987**, *184*, 1.
(15) Bolding, B. C.; Carter, E. A. *Phys. Rev. B* **1991**, *44*, 3251.
(16) Tong, W. M.; Snyder, E. J.; Williams, R. S.; Yanase, A.; Segawa, Y.; Anderson, M. S. *Surf. Sci.* **1992**, *277*, L63.
(17) Grabow, M. H.; Gilmer, G. H. *Surf. Sci.* **1988**, *194*, 333.
(18) Grabow, M. H.; Gilmer, G. H. *Mat. Res. Soc. Symp. Proc.* **1987**, *94*, 15.
(19) Raeker, T. J.; DePristo, A. E. *Surf. Sci.* **1991**, *248*, 134.
(20) Dodson, B. W.; Taylor, P. A. *Phys. Rev. B* **1986**, *34*, 2112.
(21) Taylor, P. A.; Dodson, B. W. *Phys. Rev. B* **1987**, *36*, 1355.
(22) Faux, D. A.; Gaynor, G.; Carson, G. L.; Hall, C. K.; Bernholc, J. *Phys. Rev. B* **1990**, *42*, 2914.
(23) Bolding, B. C.; Carter, E. A. *Phys. Rev. B* **1990**, *42*, 11380.
(24) Luedtke, W. D.; Landman, U. *Phys. Rev. B* **1991**, *44*, 5970.
(25) Chang, T.-M.; Carter, E. A. *Surf. Sci.* **1994**, *318*, 187.
(26) Li, Y. S.; Quinn, J.; Li, H.; Tian, D.; Jona, F.; Marcus, P. M. *Phys. Rev. B* **1991**, *44*, 8261.
(27) Li, H.; Wu, S. C.; Tian, D.; Li, Y. S.; Quinn, J.; Jona, F. *Phys. Rev. B* **1991**, *44*, 1438.
(28) Han, M.; Mrozek, P.; Wieckowski, A. *Phys. Rev. B* **1993**, *48*, 8329.
(29) Polanski, G.; Toennies, J. P. *Surf. Sci.* **1992**, *260*, 250.
(30) Takayanagi, K. *Surf. Sci.* **1981**, *104*, 527.
(31) Bolding, B. C.; Carter, E. A. *Surf. Sci.* **1992**, *268*, 142.
(32) Carter, L. E.; Weakliem, P. C.; Carter, E. A. *J. Vac. Sci. Technol. A* **1993**, *11*, 259.
(33) Dodson, B. W. *Phys. Rev. B* **1984**, *30*, 3545.
(34) Press, W. H.; Flannery, B. P.; Teukosky, S. A.; Vetterling, W. T. *Numerical Recipes*; Cambridge University Press: Cambridge, U.K., 1989.
(35) Xu, R.; Bao, S.; Liu, G. *Surf. Sci.* **1990**, *234*, 335.
(36) Schmitz, P. J.; Leung, W. Y.; Thiel, P. A. *Phys. Rev. B* **1989**, *40*, 11477.
(37) Finnis, M. W.; Sinclair, J. E. *Philos. Mag. A* **1984**, *50*, 45.
(38) Sutton, A. P.; Chen, J. *Philos. Mag. Lett.* **1990**, *61*, 139.
(39) Rafii-Tabar, H.; Sutton, A. P. *Philos. Mag. Lett.* **1991**, *63*, 217.
(40) Todd, B. D.; Lynden-Bell, R. M. *Surf. Sci.* **1993**, *281*, 191.
(41) Koleske, D. D.; Sibener, S. J. *Surf. Sci.* **1993**, *290*, 179.
(42) Black, J. E. *Phys. Rev. B* **1992**, *46*, 4292.
(43) Radeke, M. R.; Carter, E. A. *Phys. Rev. B* **1995**, *51*, 4388.
(44) Shiang, K.-D.; Tsong, T. T. *Phys. Rev. B* **1995**, *March 15*.
(45) Van Hove, M. A.; Weinberg, W. H.; Chan, C.-M. *Low-Energy Electron Diffraction*; Springer-Verlag: Berlin, 1986; p 256.
(46) Raeker, T. J.; DePristo, A. E. *Surf. Sci.* **1994**, *310*, 337.
(47) Flynn-Sanders, D. K.; Evans, J. W.; Thiel, P. A. *Surf. Sci.* **1993**, *289*, 75.
(48) Macur, J. E.; Vook, R. W. *Thin Solid Films* **1980**, *66*, 371.
(49) Wytenburg, W. J.; Ormerod, R. M.; Lambert, R. M. *Surf. Sci.* **1993**, *282*, 205.
(50) Eisenhut, B.; Stober, J.; Rangelov, G.; Fauster, Th. *Phys. Rev. B* **1993**, *47*, 12980.
(51) Davies, P. W.; Quinlan, M. A.; Somorjai, G. A. *Surf. Sci.* **1982**, *121*, 290.
(52) Schmiedeskamp, B.; Kessler, B.; Vogt, B.; Heinzmann, U. *Surf. Sci.* **1989**, *223*, 465.
(53) Takayanagi, K.; Kolb, D. M.; Kambe, K.; Lehmpfuhl, G. *Surf. Sci.* **1980**, *100*, 407.
(54) Henrion, J.; Rhead, G. E. *Surf. Sci.* **1972**, *29*, 20.
(55) Barthès, M.; Rhead, G. E. *Surf. Sci.* **1979**, *80*, 421.

JP941983N